

Article

Persistent Meteorological Drought in the Yangtze River Basin during Summer–Autumn 2022: Relay Effects of Different Atmospheric Internal Variabilities

Ruili Wang^{1,2,3}, Xiao Li^{2,4,*}, Hedi Ma^{1,2,*}, Xing Li⁴ , Junchao Wang¹ and Anwei Lai¹

¹ China Meteorological Administration Basin Heavy Rainfall Key Laboratory/Hubei Key Laboratory for Heavy Rain Monitoring and Warning Research, Institute of Heavy Rain, China Meteorological Administration, Wuhan 430205, China; wangrl_06@163.com (R.W.); wangjunchao@whihr.com.cn (J.W.); laianwei@whihr.com.cn (A.L.)

² Key Laboratory of Meteorological Disaster (KLME), Ministry of Education & Collaborative Innovation Center on Forecast and Evaluation of Meteorological Disasters(CIC-FEMD), Nanjing University of Information Science & Technology, Nanjing 210044, China

³ Wuhan Meteorological Observatory, Wuhan 430040, China

⁴ Plateau Atmosphere and Environment Key Laboratory of Sichuan Province, College of Atmospheric Science, Chengdu University of Information Technology, Chengdu 610225, China; lx_cuit@163.com

* Correspondence: lixiao@cuit.edu.cn (X.L.); mahedi@whihr.com.cn (H.M.)

Abstract: During the summer–autumn (July–October, Jul–Oct) period of 2022, the Yangtze River Basin (YRB) of China experienced an extreme meteorological drought, with Jul–Oct containing the lowest precipitation in the YRB since 1979. The possible causes of this drought were analyzed in the present study. Surprisingly, unlike many previous drought events, we found that this event was not characterized by a consistent atmospheric circulation anomaly regime throughout the entire drought period. Instead, two distinct circulation patterns were responsible for the precipitation deficit in two different stages, i.e., July–August (Jul–Aug) and September–October (Sep–Oct). In Jul–Aug, the YRB precipitation deficit primarily resulted from an intensified and northward-shifted East Asian subtropical jet, which allowed for an extremely northwestward shift of western Pacific subtropical highs, leading to an anomalous descending motion. Such circulation patterns in Jul–Aug originated from the dispersion of Rossby waves upstream from central Asia and Europe. Meanwhile, in Sep–Oct, the YRB drought was primarily attributed to a low-level cyclonic anomaly over the western North Pacific, which was closely associated with frequent tropical cyclones traveling across this region. Observational analysis and a model ensemble hindcast suggest that atmospheric internal variabilities dominated the drought process, while the SSTA, particularly the La Niña event, played a limited role. Therefore, this long-lasting extreme YRB meteorological drought was largely driven by the relay effects of different atmospheric internal variabilities in Jul–Aug and Sep–Oct, respectively, which shows limited model predictability and poses a great challenge for operational climate predictions.

Keywords: meteorological drought; atmospheric internal variability; La Niña event; wave train



Citation: Wang, R.; Li, X.; Ma, H.; Li, X.; Wang, J.; Lai, A. Persistent Meteorological Drought in the Yangtze River Basin during Summer–Autumn 2022: Relay Effects of Different Atmospheric Internal Variabilities. *Atmosphere* **2023**, *14*, 1402. <https://doi.org/10.3390/atmos14091402>

Academic Editors: Yuqing Zhang and Jianyu Liu

Received: 22 July 2023

Revised: 24 August 2023

Accepted: 29 August 2023

Published: 5 September 2023



Copyright: © 2023 by the authors. Licensee MDPI, Basel, Switzerland. This article is an open access article distributed under the terms and conditions of the Creative Commons Attribution (CC BY) license (<https://creativecommons.org/licenses/by/4.0/>).

1. Introduction

The Yangtze River Basin (YRB) is located in the East Asian monsoon region. With urbanization and population growth, water resources have become a crucial factor in the sustainable development of the YRB [1]. Unfortunately, YRB precipitation (YRBP) exhibits strong variation at multiple timescales, leading to frequent drought and flood disasters in this region [2]. Thus, understanding the causes of YRB drought is important not only for the scientific community but also for operational climate centers.

Great effort has been devoted to discerning the possible causes of droughts in the YRB region. Studies have demonstrated that persistent external forces, for example, the sea surface temperature anomaly (SSTA) in the tropical oceans, convection anomalies over

the Indo-Pacific warm pool, anomalous soil moisture, and snow cover over the Eurasian continent, as well as the Arctic sea ice anomaly, play important roles in YRB droughts through changing the atmospheric circulation patterns [3–7]. Atmospheric internal variabilities such as the East Asia–Pacific pattern, the Eurasian teleconnection pattern, and changes to the western Pacific subtropical high (WPSH) and the East Asian subtropical jet (EASJ) have been shown to contribute directly to precipitation anomalies in the YRB [8–11]. However, the mechanisms of YRB drought events usually involve interactions among multiple climate factors and thus exhibit a large degree of complexity [12].

In the summer of 2022, the YRB region suffered from an extraordinarily severe meteorological drought, concurrent with extreme heat waves. Many existing studies have focused on the possible causes underlying this drought. These studies attributed the extreme event to both external forces and internal variabilities, for example, the anthropogenic warming background [13], the La Niña event [14], thermal anomalies over the Tibetan Plateau [15], as well as circulation patterns across the Eurasian continent [16]. However, although the heat wave was alleviated, the meteorological drought in the YRB region did not show any signs of mitigation in the subsequent autumn, thus giving rise to a severe summer–autumn persistent drought event (Figure 1). The long-lasting drought caused the Yangtze River to exhibit an extremely low water level, which resulted in severe water scarcity and huge agricultural losses. However, up to now, insufficient attention has been paid to discovering how this extreme drought could have lasted from summer to autumn.

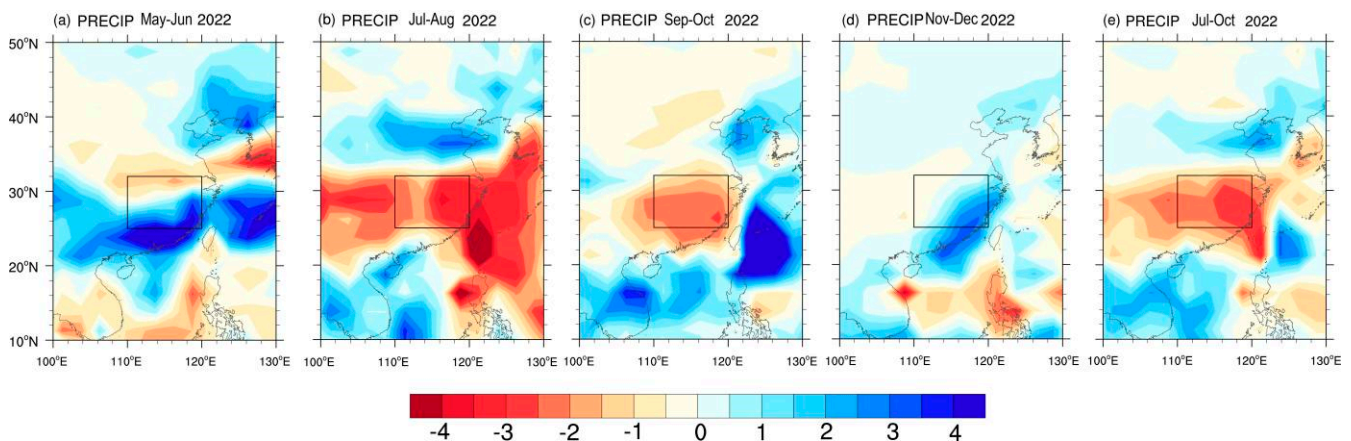


Figure 1. (a–d) show the spatial distributions of bi-monthly anomalous precipitation (units: mm/day) in May–June (May–Jun), July–August (Jul–Aug), September–October (Sep–Oct), and November–December (Nov–Dec) of 2022, respectively. (e) shows July–October (Jul–Oct) mean precipitation anomaly (units: mm/day).

To discover the dynamical causes of historical persistent droughts, most studies emphasize the role of long-lasting atmospheric circulation anomaly patterns [17–20]. However, we noted that the regime of circulation had experienced a substantial shift during the drought process of 2022, hinting that this YRB drought may be attributed to different reasons at different stages, which may be a unique feature that deserves further investigation. Therefore, in this study, we attempt to investigate the possible causes of this long-lasting drought, as well as to discuss its potential predictability. Particularly, we mainly focus on the following two objectives: (a) What are the dominant climate factors driving this persistent drought at different stages? (b) What are the roles of atmospheric internal variabilities and external forces, particularly the triple-dip La Niña event? Section 2 provides a description of the datasets and methods used in this study. The precipitation deficit and the physical mechanisms are discussed in Sections 3 and 4. Section 5 provides a summary and discussion.

2. Data and Methods

The monthly precipitation dataset from the Global Precipitation Climatology Project (GPCP) with a horizontal resolution of $2.5^\circ \times 2.5^\circ$ was used in this study [21]. The Centennial in situ Observation-Based Estimates dataset of SST, which has a resolution of $1.0^\circ \times 1.0^\circ$, was also employed [22]. For the circulation variables, we used the National Centers for Environmental Prediction–Department of Energy (NCEP-DOE) atmospheric reanalysis dataset [23], with a horizontal resolution of $2.5^\circ \times 2.5^\circ$. Considering that the observations and reanalysis before the satellite era (around 1979) exhibit larger uncertainties, the analysis period of the present study ranges from 1979 to 2022. We employed tropical cyclone (TC) best-track data from the China Meteorological Administration [24], which has a horizontal resolution of $0.1^\circ \times 0.1^\circ$.

The present study used the real-time predictions from the NCEP Climate Forecast System Version 2 (NCEP CFSv2). The NCEP CFSv2 is a state-of-the-art fully coupled atmosphere–ocean–land model, incorporating detailed representations of the atmospheric, oceanic, sea ice, and land components. It employs a high horizontal resolution of T126 with 64 vertical hybrid sigma-pressure levels in the atmosphere. The advanced subgrid-scale physical parameterizations realistically simulate processes like radiation absorption and emission, cloud formation and dissipation (including stratus, stratocumulus and cumulus), turbulent mixing in the planetary boundary layer, as well as a complex formulation of precipitation processes. Ensemble means of real-time predictions initiated in May 2022 from the NCEP CFSv2 were examined in this work to investigate the predictability of this drought event. This system generated 124 ensemble members through perturbing the initial conditions using the final states from the preceding month (i.e., May), with 4 members produced per day, which contained 124 members. In this study, climate anomalies were defined as the deviations from the climatological mean of 1982–2010, consistent with the hindcast period of CFSv2.

The Niño 3.4 index was defined as the averaged SST anomaly over $170^\circ\text{--}120^\circ\text{ W}$, $5^\circ\text{ S--}5^\circ\text{ N}$. La Niña events were defined based on a threshold of -0.5° C of the Niño 3.4 index for Jul–Oct. According to this definition, 13 La Niña years were identified, including 1985, 1989, 1995, 1998, 1999, 2000, 2007, 2010, 2011, 2016, 2020, 2021, and 2022. The Niño 3.4 index had been demonstrated to effectively identify El Niño and La Niña events [25]. Other indices, for example, the Oceanic Niño Index and the Multivariate El Niño Index, are also effective indicators of El Niño and La Niña, but we noted our results were not quite sensitive to the chosen index. To describe the propagation of Rossby wave energy in the upper troposphere, the phase-independent wave activity flux (WAF) was calculated [26]. The WAF is parallel to the group velocity of local Rossby waves; thus, it represents the propagation of the wave packet.

3. The Summer–Autumn Persistent Precipitation Deficit

Figure 1a–d show the bi-monthly precipitation anomalies in central-eastern China during 2022. In May–June (May–Jun, Figure 1a), precipitation was above (below) normal in southern (northern) part of the YRB region. But in July–August (Jul–Aug, Figure 1b) and September–October (Sep–Oct, Figure 1c), most of the YRB had experienced persistent precipitation deficits. The strongest precipitation deficit occurred over the southeastern part of the YRB, exceeding -3.5 mm/day in Jul–Aug and -2.5 mm/day in Sep–Oct. Figure 1e shows the July–October (Jul–Oct) precipitation anomaly; the precipitation deficit almost occupied the entire YRB region during this period. The precipitation rate over the domain of $25^\circ\text{--}32^\circ\text{ N}$, $110^\circ\text{--}120^\circ\text{ E}$ in Jul–Oct was only about 1.9 mm/day , less than half the climatological value (about 4.2 mm/day). In this study, we defined a YRBP index (YRBPI) as precipitation anomalies averaged over the domain of $25^\circ\text{--}32^\circ\text{ N}$, $110^\circ\text{--}120^\circ\text{ E}$ (the black rectangle in Figure 1). Figure 2a–c show the normalized YRBPI in Jul–Aug, Sep–Oct and Jul–Oct, respectively, they all reached the lowest value since 1979 in 2022. In November–December (Nov–Dec, Figure 1d), above-normal precipitation appeared over

most of the YRB, hinting at the mitigation of the drought. We hereinafter focused on Jul–Oct to investigate this YRB drought event.

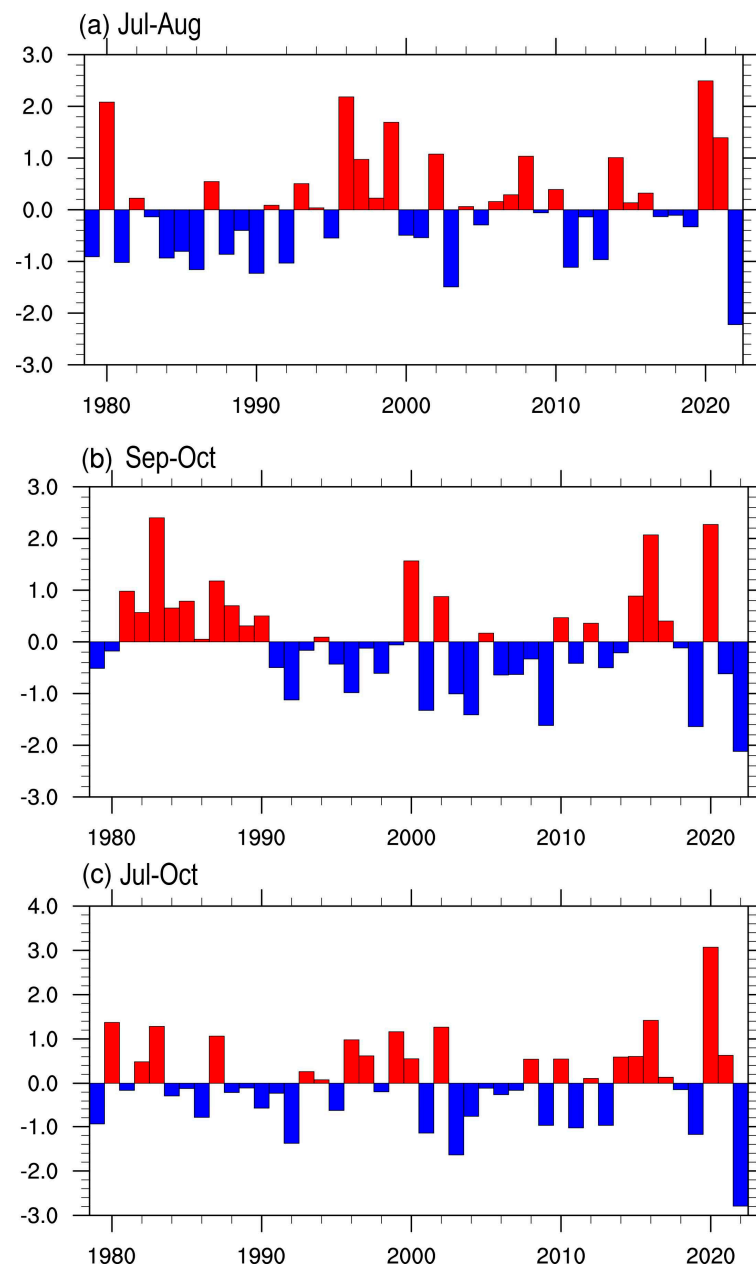


Figure 2. Time series of the normalized YRBPI (averaged over $110\text{--}120^\circ$ E and $25\text{--}32^\circ$ N, as shown in the black box in Figure 1) from 1979 to 2022 for Jul–Aug (a), Sep–Oct (b), and Jul–Oct (c).

4. The Physical Causes of the Persistent Drought

4.1. Seasonal Change of Circulation Regime Associated with Drought

Although this drought persisted from summer to autumn, the associated atmospheric circulation patterns exhibited very distinct features in different seasons. Figure 3a shows Jul–Aug’s mean 500 hPa geopotential height (GPH) and 850 hPa wind. It was found under the influence of a summer monsoon; a branch of low-level southerly appeared over central-eastern China, transporting abundant moisture from tropical oceans and leading to enhanced 850 hPa moisture over most of central-eastern China (Figure 3c). But the YRB had still received very limited rainfall due to the control of WPSH at 500 hPa (Figure 3a). As indicated from Figure 3a, the WPSH in Jul–Aug 2022 was stronger and located far more westward than in the climatology, which resulted in an anomalous descending motion

at 500 hPa (Figure 3c) and thus suppressed the YRBP. However, the circulation regime in autumn 2022 was very different. In Sep–Oct, although the 500 hPa WPSH was still stronger than normal, it had retreated southward to south China due to season evolution, leaving the YRB located to the northern edge of the WPSH (Figure 3b), which was supposed to enhance precipitation over the YRB. But there was still very limited rainfall because the low level of central-eastern China had shifted to a northerly regime that reduced local moisture and had caused a descending motion (Figure 3b,d). The remarkably different low-level circulation and moisture anomaly in Jul–Aug and Sep–Oct 2022 suggested that the drought may have had disparate attributions in different seasons, which should be discussed separately. Subsequently, we show our analysis of the physical mechanisms relating to the precipitation anomaly for Jul–Aug and Sep–Oct, respectively.

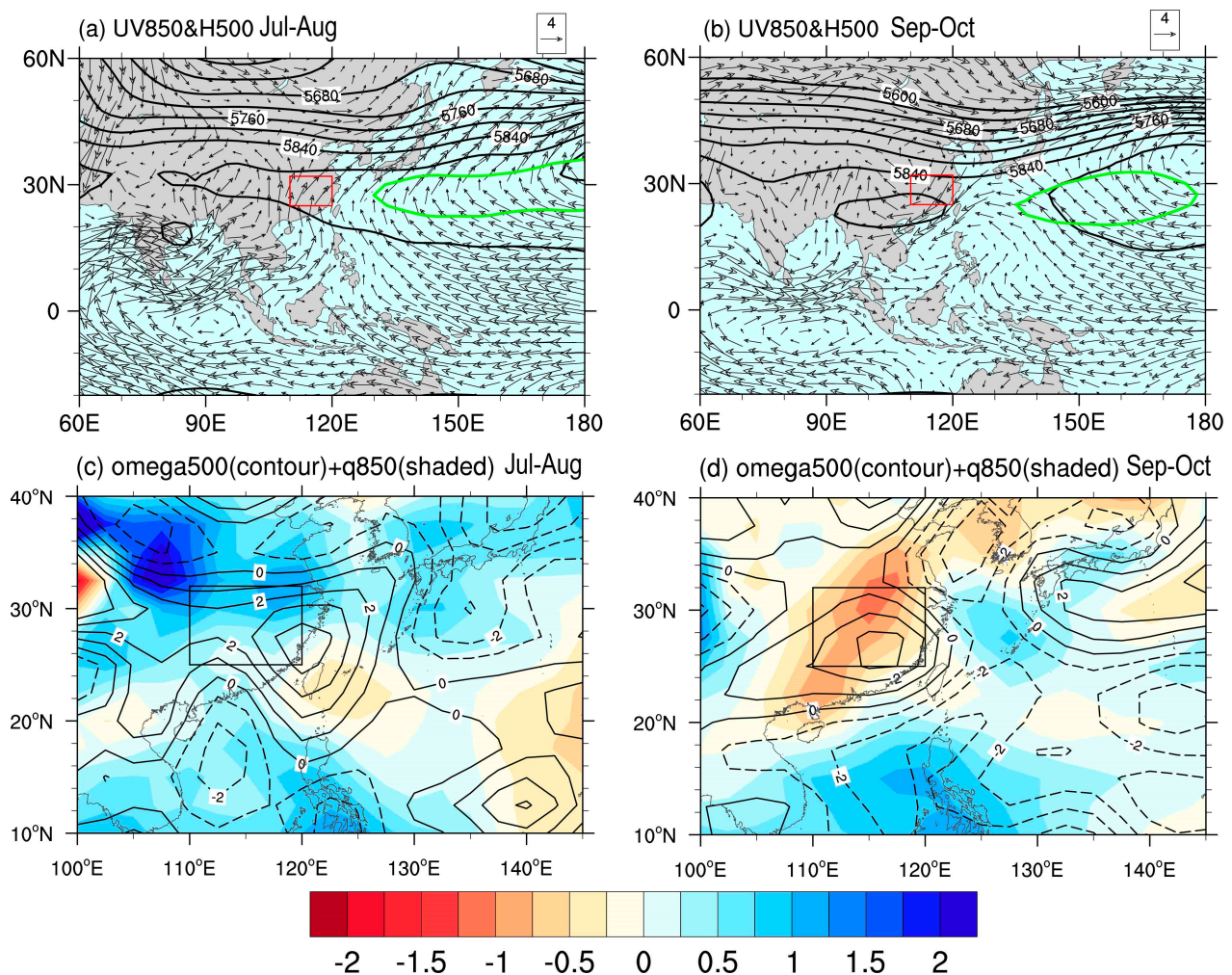


Figure 3. (a,b) are the mean field of the 500 hPa geopotential and 850 hPa wind in Jul–Aug and Sep–Oct of 2022, respectively; green contour denotes climatological 5880 gpm isoline. (c,d) show the observed 850 hPa specific humidity (shading, g kg^{-1}) and 500 hPa vertical velocity (contour, $-\text{0.01 Pa s}^{-1}$) anomalies in Jul–Aug and Sep–Oct of 2022.

4.2. The Causes of Jul–Aug Drought

To better document the reason for the 2022 summer precipitation anomaly over the YRB, we compared the atmospheric circulation anomaly in 2022 with that associated with the typical dry YRBP anomalies. The regressed wind vector at 850 hPa and sea level pressure (SLP) against the negative YRBP in Jul–Aug are depicted in Figure 4a. For the dry anomaly in the YRB, there were cyclonic anomalies over the subtropical western North Pacific (WNP) and northeastern Asia (NEA). These wind anomalies diverged over

the YRB and were unfavorable for rainfall there. It is noted that the cyclonic anomalies over NEA were statistically significant, while the cyclonic anomalies over the WNP were only with marginal significance, suggesting the mid-latitude circulation anomalies may play more important role than tropical circulation anomalies in affecting Jul–Aug YRBP variability. The observed 850 hPa wind and SLP anomalies in Jul–Aug 2022 are shown in Figure 4b. The tropical circulation pattern at 850 hPa in Jul–Aug 2022 was quite distinct from the historical perspective. Instead of an anomalous cyclone, there existed a giant anomalous anticyclone over the WNP, enhancing southwesterly moisture transport to the YRB. Therefore, the observed low-level WNP circulation anomaly was unable to explain the extreme YRB drought in Jul–Aug 2022. Meanwhile, a large-scale low-pressure anomaly dominated the NEA region (Figure 4b), consistent with the historical perspective, which would suppress the cold northeasterly and frontogenesis over the YRB and thus contribute to the dry anomaly [8].

Further, we analyzed the impacts of upper tropospheric circulation anomalies on the YRBP. The regressed 250 hPa wind and GPH anomalies against the negative YRBPI are depicted in Figure 4c. For the dry Jul–Aug period, circulation over East Asia featured a meridional dipole pattern. An anticyclonic anomaly existed over central-eastern China, while cyclonic anomaly extended from Siberia to NEA. Between them, westerly wind increased significantly at 40–45° N over East Asia, corresponding to an intensified and northward shifted EASJ, in agreement with the findings of many previous studies [27,28]. To further characterize this EASJ anomaly, an EASJ index (EASJI) was defined as the normalized 250 hPa zonal wind anomalies averaged over 40–45° N, 100–140° E. The correlation coefficient between the EASJI and the YRBPI during 1979–2022 reaches -0.56 ($p < 0.01$), demonstrating a close linkage between EASJ and YRBP. In Jul–Aug 2022, the 250 hPa circulation anomalies over East Asia resembled the regressed pattern (Figure 4d), and the EASJI reached 2.29, the highest since 1979 (Figure 4e). Thus, the strengthening and northward shift of EASJ was very crucial to the summer YRB drought of 2022, which allowed for an extremely northwestward shift of WPSH, leading to an anomalous descending motion (Figure 3a,e). Li et al. [8] pointed out the strengthening and meridional displacement of the EASJI is typically accompanied by a cyclonic anomaly over NEA in the lower troposphere, consistent with the pattern in Figure 4b.

Then, it comes naturally to ask, what are the physical mechanisms of drought for Jul–Aug? To see whether the SSTA played a role, Figure 5a shows regressed Jul–Aug SSTA onto the YBPI. Associated with the Jul–Aug rainfall deficit, the eastern Indian Ocean, south China Sea, and Philippine Sea showed significant cooling. As shown in Figure 4a, the Jul–Aug rainfall deficit in the YRB was accompanied by cyclonic anomalies over these oceans. Therefore, the observed SST cooling may reflect an atmospheric force on the ocean, rather than the opposite. In other ocean basins, very limited significant signals were detected. Notably, SSTA in Jul–Aug 2022 featured a La Niña-like pattern (Figure 5b). To investigate the potential effects of La Niña events, the composite anomalies of SLP and wind vector at 850 hPa for 12 historical La Niña events (excluding 2022) are displayed in Figure 6a. In Jul–Aug, the La Niña-associated central Pacific cooling would favor the WNP anticyclone anomaly via the Gill-type Rossby wave response. Consequently, the southwesterly to the northwestern flank of the anticyclone would lead to a slight wet anomaly in the YRB region (Figure 6a). Therefore, the observed remarkable WNP anticyclone anomaly in Jul–Aug 2022 was possibly due to the La Niña forcing, but it was unable to explain the observed negative YRBP anomaly. In addition, the La Niña-associated 250 hPa wind and GPH anomalies were distinct from those in Jul–Aug 2022 (Figures 4d and 6b), suggesting the La Niña event was also less likely to impact the observed YRBP in 2022 through modulating the EASJ anomaly.

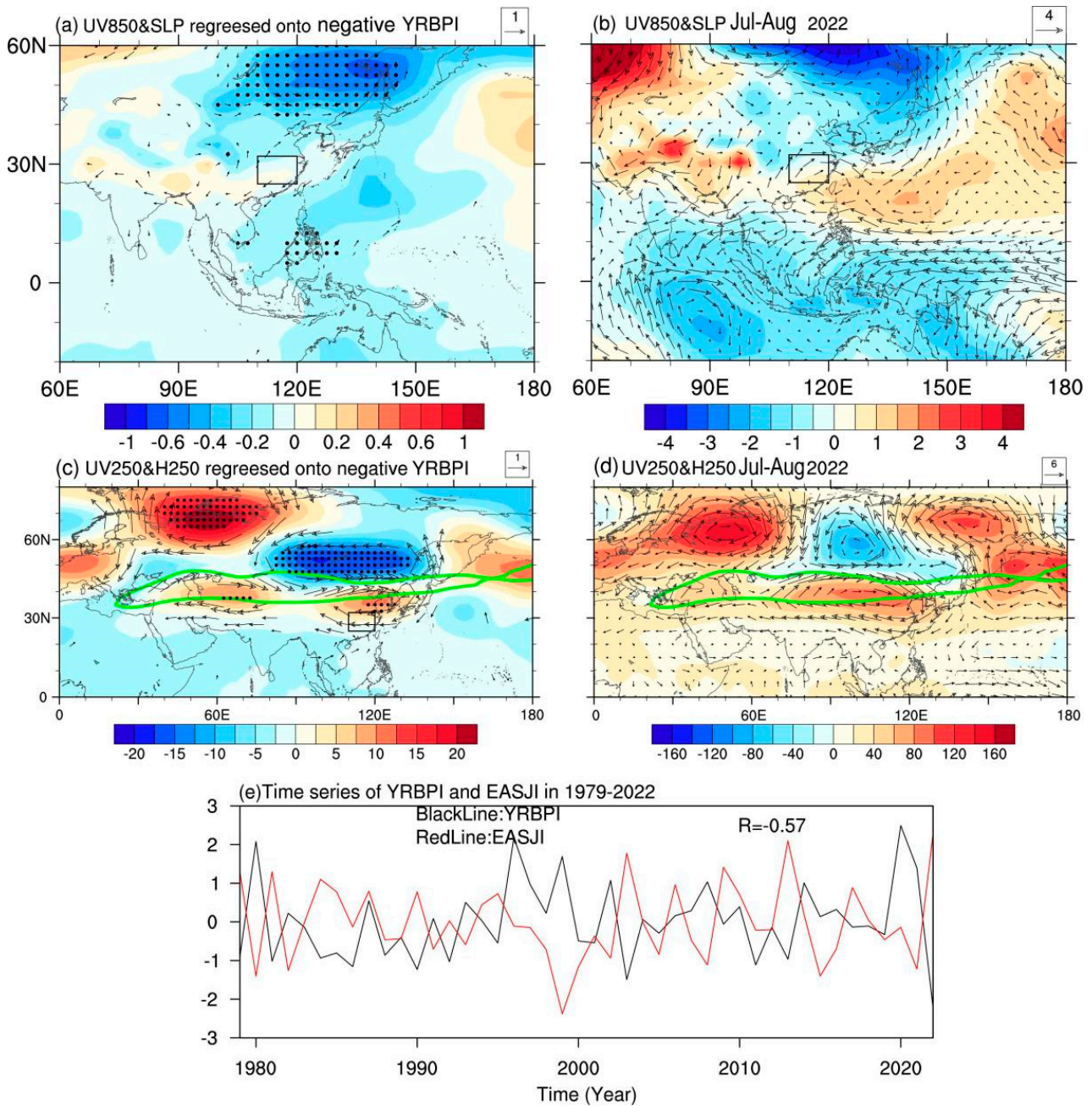


Figure 4. (a) Regression map of sea level pressure (SLP) anomalies (shading, unit: hPa) and 850 hPa wind anomalies (vector, unit: m/s; only vectors with a u or v component significant at the 95% confidence level were plotted) against the negative YRBPI in Jul–Aug for the period of 1979–2022. (b) Spatial distribution of the sea level pressure anomalies (shading, unit: hPa) and 850 hPa wind anomalies (vector, unit: m/s) in Jul–Aug 2022. (c) Regression map of the 250 hPa geopotential height anomalies (shading, unit: gpm) and 250 hPa wind anomalies (vector, unit: m/s, only vectors with a u or v component significant at the 95% confidence level were plotted) against the negative YRBPI in Jul–Aug for the period of 1979–2022. Dotted areas denote the 95% confidence level based on the two tailed Student’s *t* test. (d) Spatial distribution of the 250 hPa geopotential height anomalies (shading, unit: gpm) and 250 hPa wind anomalies (vector, unit: m/s) in Jul–Aug 2022. (e) Normalized time series of YRBPI and EASJI in Jul–Aug.

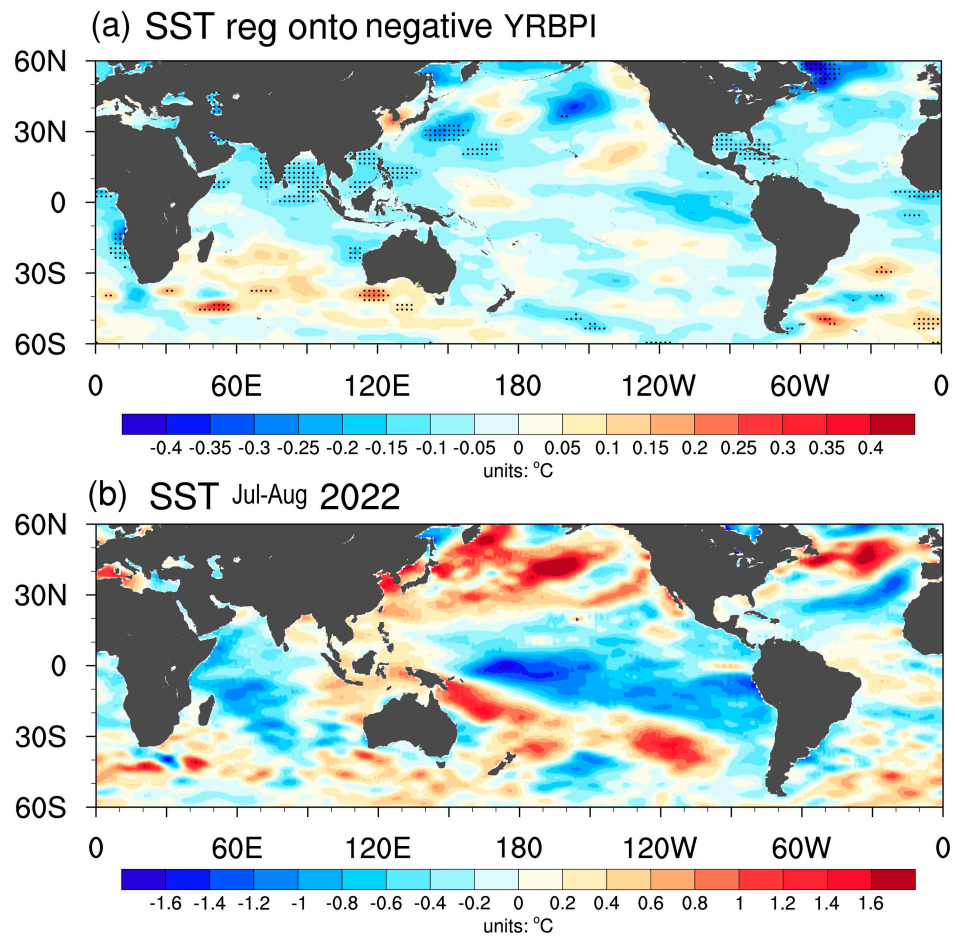


Figure 5. (a) Regression map of SST (unit: °C) against the negative YRBPI in Jul–Aug for the period of 1979–2022. Dotted areas denote the 95% confidence level based on the two-tailed Student’s *t* test. (b) Spatial distribution of detrended SST (unit: °C) anomalies in Jul–Aug 2022.

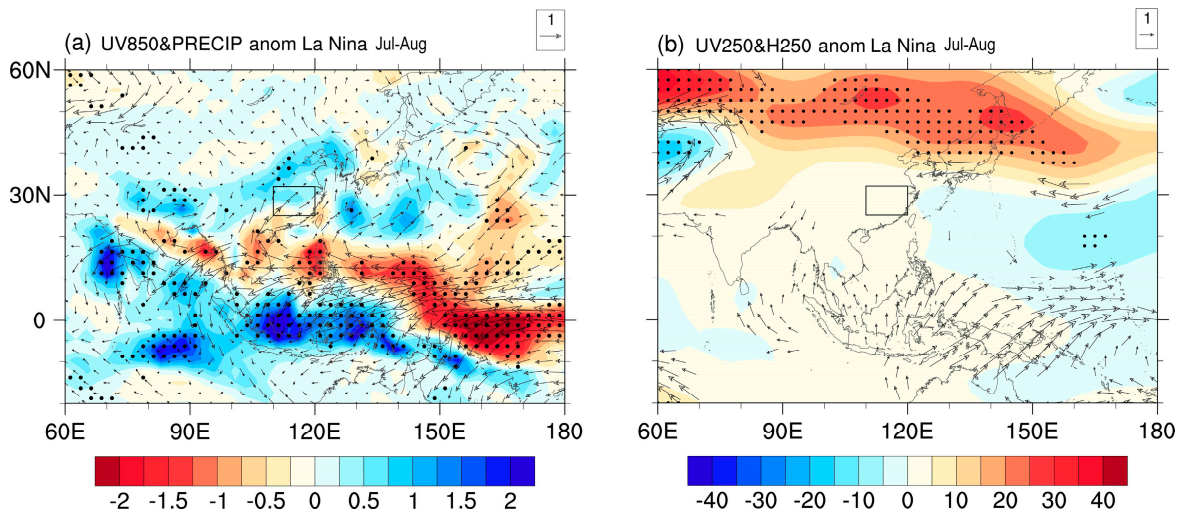


Figure 6. (a) shows the composite of the precipitation anomalies (shading, unit: mm/day) and 850 hPa wind anomalies (vector, unit: m/s, only vector with *u* or *v* component significant at the 95% confidence level was plotted) of 12 historical La Niña events in Jul–Aug. (b) shows the composite of the 250 hPa GPH anomalies (shading, unit: gpm) and 250 hPa wind anomalies (vector, unit: m/s, only vector with *u* or *v* component significant at the 95% confidence level was plotted) of 12 historical La Niña events in Jul–Aug.

Our further analysis demonstrated the mid-to-high latitude circulation anomalies over EA were due to Rossby wave patterns across the Eurasian continent. Figure 7a,b separately show the 250-hPa GPH anomalies and the corresponding WAFs for July and August 2022. Upstream Rossby wave energy propagation towards East Asia was seen in both months, but with different paths. In July, the WAFs originated from the anticyclone over central Asia, propagated northeastward to Lake Baikal, and then turned southeastward to central-eastern China. Several recent studies had attributed this pattern in July 2022 to the Rossby wave response to extremely high precipitation anomalies over India and Pakistan, which exerted an upper tropospheric anticyclone anomaly over central Asia [16]. In August, WAFs originated from the anomalous anticyclone in Europe. The wave energy first propagated southeastward to central Asia; then, it turned eastward and produced a strong anticyclone anomaly extending from northern China to central-eastern China. Afterwards, the WAFs turned northeastwards and caused cyclonic anomaly over NEA. Therefore, although upstream wave paths were different during these two months, they collectively caused the meridional dipole GPH anomaly pattern over East Asia and thus resulted in the changes in EASJ.

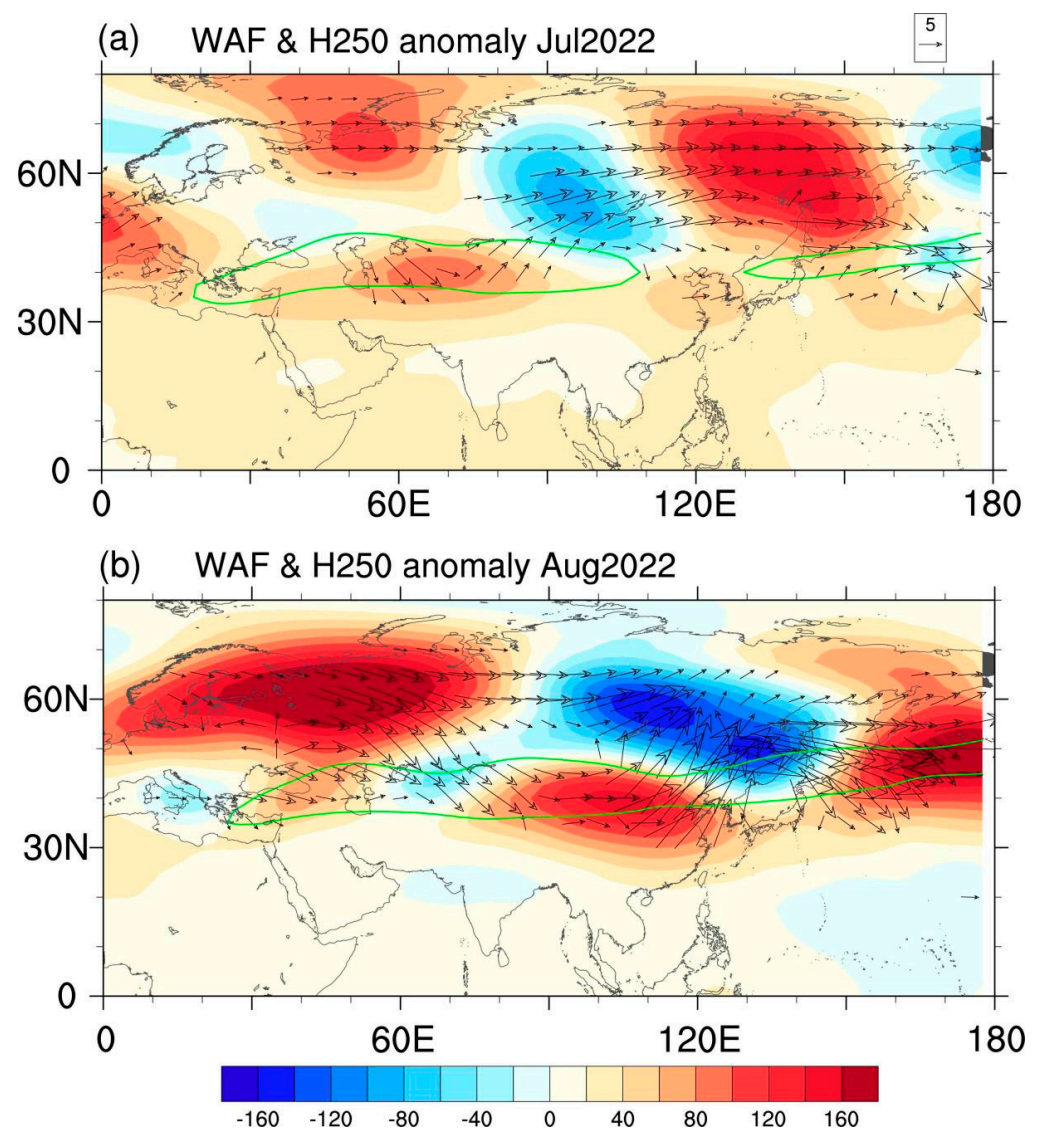


Figure 7. 250 hPa GPH anomalies and the associate WAF for (a) July and (b) August, respectively; green line denotes the 20 m/s contour of climatology Asian westerly jet.

4.3. The Causes of Sep–Oct Drought

In this section, we compared the atmospheric circulation anomaly in 2022 with that associated with the typical dry YRBP anomalies in Sep–Oct. The regressed wind vector at 850 hPa and SLP against the negative YRBP in Sep–Oct is depicted in Figure 8a. Associated with the Sep–Oct drought, large-scale low pressure and cyclonic anomalies appeared over the WNP. Specifically, a significant northerly extended from southeastern China to the Philippine Islands, unfavorable for moisture transport from tropical oceans to the YRB, thus causing negative rainfall anomalies. The observed 850 hPa wind and SLP anomaly in Sep–Oct 2022 is shown in Figure 8b, which was reasonably similar to the regression pattern given in Figure 8a. A strong cyclonic anomaly occurred over the WNP region. To its western flank, an evident northerly anomaly over southeastern China weakened the moisture transport from the tropical oceans. To reveal the effects of the northerly to the western flank of the WNP cyclone, a WNP meridional wind index (WNPVI) was defined as normalized 850 hPa meridional anomalies averaged over 10–25° N, 110–130° E, as shown in Figure 8e. The correlation coefficient between YRBP and WNPVI reaches 0.54 ($p < 0.01$); the WNPVI in Sep–Oct 2022 was -1.78 , the lowest since 1979, demonstrating the northerly to the western flank of WNP cyclone played an important role in the YRB drought of Sep–Oct 2022. This was also consistent with several previous findings emphasizing the role of a WNP cyclone in triggering the autumn drought in the YRB region [29]. However, the impact from upper tropospheric circulation anomaly was relatively rigorous. The regressed pattern suggested dry anomaly over the YRB is associated with a large cyclonic anomaly over central-eastern China (Figure 8c). But in the dry event of Sep–Oct 2022 (Figure 8d), the central-eastern China was dominated by an anticyclonic anomaly, distinct with its historical perspective. The above analysis suggests that, unlike the drought in Jul–Aug 2022, the precipitation deficit in Sep–Oct was mainly attributed to a low-level cyclonic anomaly over the WNP region. Then, it comes naturally to ask what caused the low-level cyclone anomaly over the WNP region. Does it relate to SSTA, particularly the La Niña event?

To see the effects of SSTA, we show regressed Sep–Oct SSTA onto the YRBP in Figure 9a. Associated with rainfall deficit in Sep–Oct, the central Pacific showed significant warming, which was nearly opposite to the SSTA pattern in Sep–Oct 2022 that featured a La Niña-like pattern (Figure 9b). From the historical perspective, La Niña SSTA during Sep–Oct would induce an anticyclone anomaly located in the WNP (Figure 10a), while the South China Sea was occupied by a cyclonic anomaly. Such a circulation pattern induced a southeasterly anomaly towards central-eastern China, which led to a weak positive YRBP anomaly (Figure 10a). These results are consistent with a finding of Hu et al. [30]. We noted that in Sep–Oct 2022, the WNP was occupied by a giant cyclonic anomaly (Figure 8b), with an anomalous northerly and precipitation deficit observed in the YRB. These anomalies in Sep–Oct 2022 were also quite different from those of historical La Niña events, suggesting the La Niña event was less likely to cause the WNP cyclone and the YRBP deficit in Sep–Oct 2022. So why did the La Niña autumn of 2022 exhibit a cyclone anomaly rather than an anticyclone anomaly over the WNP? Further analysis suggested synoptic disturbances may play a role, particularly tropical cyclone (TC) activities. In order to explore the role of the TCs in the seasonal behavior of the WNP circulation pattern, the 61 days in Sep–Oct 2022 were classified into two groups. One was the TC group that consists of 35 days with TC activity across the WNP region. Here, the days with TC recorded that enter 10–25° N and 120–150° E during Sep–Oct 2022 were defined as TC-group days. The other was the non-TC group that consists of the remaining 26 days. Figure 11 shows the 850 hPa wind and SLP anomalies in the TC and non-TC groups. The wind and pressure pattern during TC days (Figure 11a) resembled the observed (Figure 8b) Sep–Oct mean anomaly pattern, featuring a giant WNP cyclone anomaly. Interestingly, during non-TC days (Figure 11b), a positive SLP anomaly occupied the WNP, and a southeasterly anomaly dominated central-eastern China; thus, the circulation pattern over the WNP quite resembled its historical La Niña counterparts. This indicated that when the TC days' contributions were removed, the La Niña force still dominated the circulation pattern over the WNP for Sep–Oct 2022. Therefore,

in Sep–Oct 2022, the frequent TCs might have caused the development of the anomalous cyclone over the WNP, which obscured the response of the atmospheric teleconnection to the La Niña force.

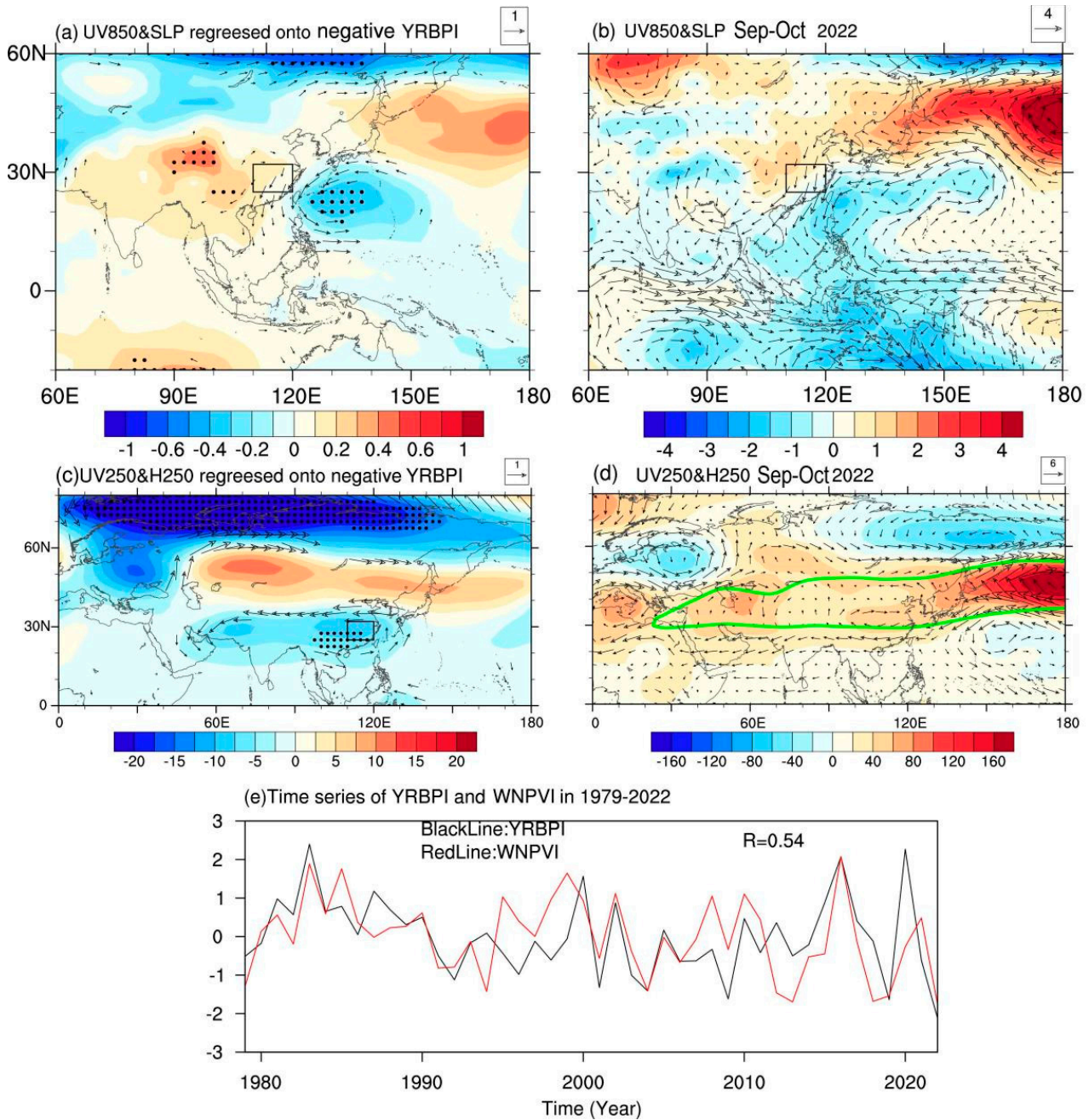


Figure 8. (a) Regression map of SLP anomalies (shading, unit: hPa) and 850 hPa wind anomalies (vector, unit: m/s, only vector with u or v component significant at the 95% confidence level was plotted) against the negative YRBPI in Sep–Oct for the period of 1979–2022. (b) Spatial distribution of the sea level pressure anomalies (shading, unit: hPa) and 850 hPa wind anomalies (vector, unit: m/s) in Sep–Oct 2022. (c) Regression map of the 250 hPa geopotential height anomalies (shading, unit: gpm) and 250 hPa wind anomalies (vector, unit: m/s, only vector with u or v component significant at the 95% confidence level was plotted) against the negative YRBPI in Sep–Oct for the period of 1979–2022. Dotted areas denote the 95% confidence level based on the two tailed Student’s *t* test. (d) Spatial distribution of the 250 hPa GPH anomalies (shading, unit: gpm) and 250 hPa wind anomalies (vector, unit: m/s) in Jul–Aug 2022. (e) Normalized time series of YBPI and WNPNI in Sep–Oct.

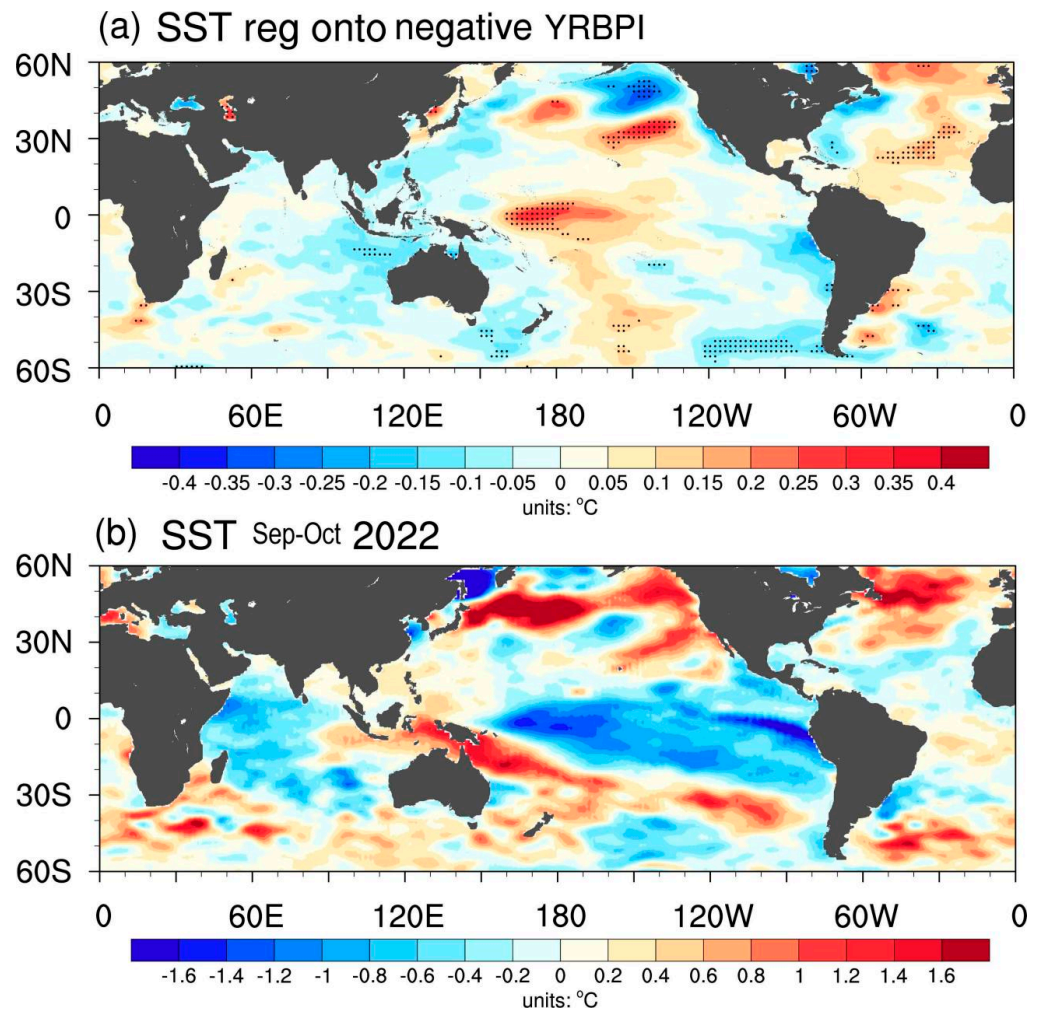


Figure 9. (a) Regression map of SST (unit: °C) against the negative YRBPI in Sep–Oct for the period of 1979–2022. Dotted areas denote the 95% confidence level based on the two-tailed Student’s *t* test. (b) Spatial distribution of SST (unit: °C) anomalies in Sep–Oct 2022.

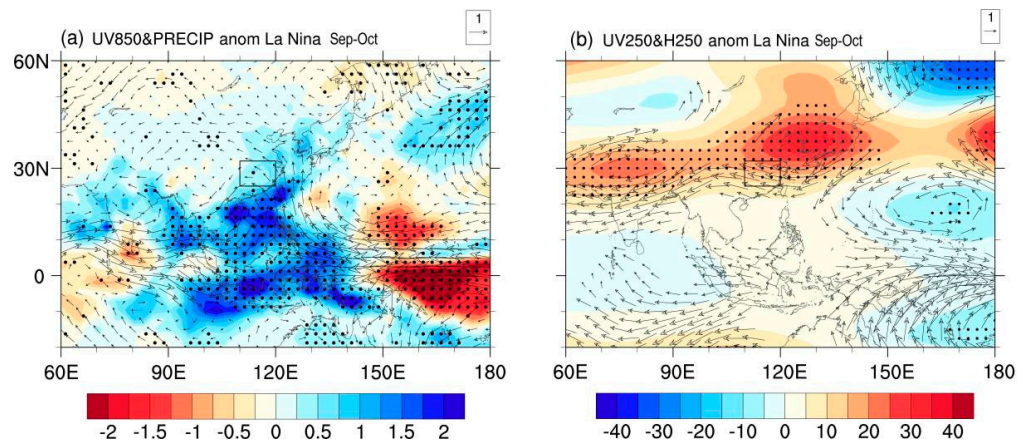


Figure 10. (a) shows the composite of the precipitation anomalies (shading, unit: mm/day) and 850 hPa wind anomalies (vector, unit: m/s, only vector with u or v component significant at the 95% confidence level was plotted) of 12 historical La Niña events in Sep–Oct. (b) shows the composite of the 250 hPa geopotential height anomalies (shading, unit: gpm) and 250 hPa wind anomalies (vector, unit: m/s, only vector with u or v component significant at the 95% confidence level was plotted) of 12 historical La Niña events in Sep–Oct.

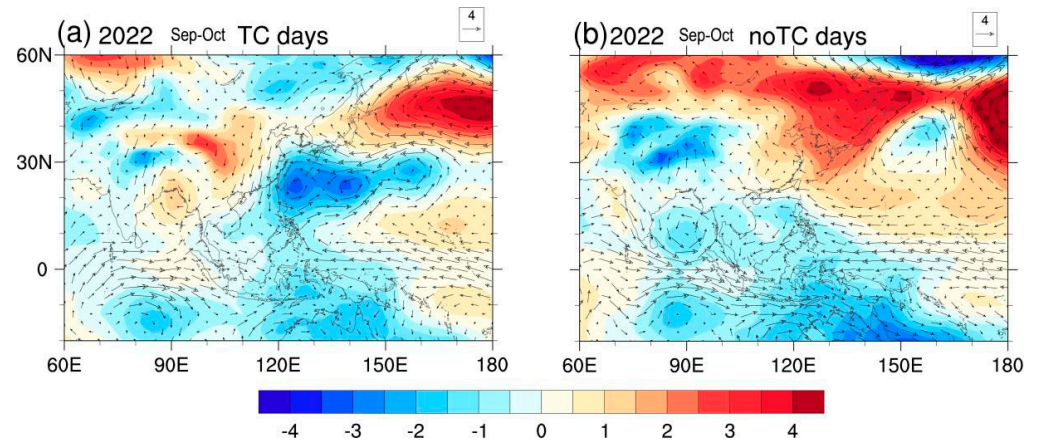


Figure 11. The composite of the sea level pressure anomalies (shading, unit: hPa) and 850 hPa wind anomalies (vector, unit: m/s) of 35 (26) days with (without) TC activity across the WNP region in Sep–Oct 2022, as shown in (a) and (b), respectively. Here, the days with TC record that enter 10–25° N and 120–150° E during Sep–Oct 2022 are defined as TC group days.

4.4. Real-Time CFSv2 Predictions

The real-time CFSv2 predictions initiated in May 2022 were displayed to examine the model predictability of this drought event. The ensemble mean (containing 124 members) of precipitation forecast failed to capture the observed severe Jul–Oct precipitation deficit in the YRB, as slightly positive rainfall anomalies appeared over most of the YRB region (Figure 12a). But it successively captured the rainfall anomalies from the tropical Indian Ocean to the tropical western Pacific (Figure 12a,c). In addition, the predicted rainfall pattern bore high resemblance to the composite La Niña rainfall pattern in tropical oceans, suggesting the ensemble mean pattern may largely reflect the effects of La Niña forcing. However, the large discrepancy between observation and model ensemble indicated that this YRB summer–autumn persistent drought was more likely caused by the atmospheric internal variability, while the SST anomalies, particularly the La Niña event, seemed not to play a key role. Interestingly, we noted that among the 124 members of the real-time forecasts of CFSv2 under the same boundary (SST) forcing, several ensemble members (e.g., member #69, Figure 12b) can well predict the YRB rainfall pattern (Figure 12c), while most of them cannot. This further demonstrated the YRB persistent drought in 2022 largely resulted from internal atmospheric dynamical processes with low predictability.

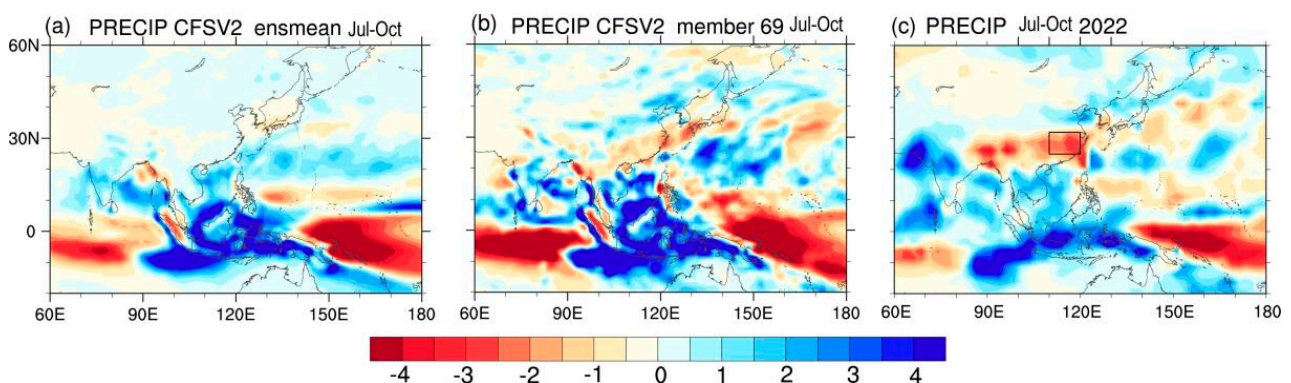


Figure 12. (a) shows CFSv2 real-time forecasts of precipitation anomalies (mm) in Jul–Oct 2022 with initial conditions in June 2022; the forecasts are 124-member ensemble mean. (b) shows forecast of precipitation anomalies (mm) in Jul–Oct 2022 from ensemble member #69. (c) shows the observed precipitation anomalies (mm) in Jul–Oct 2022.

The above analysis demonstrated that the atmospheric circulation anomaly patterns responsible for drought in Jul–Aug and Sep–Oct of 2022 were distinct. In Jul–Aug, the pattern features an intensified and northward-shifted EASJ in the upper troposphere. In Sep–Oct, the pattern featured a WNP cyclone anomaly in the lower troposphere. We found the Jul–Aug EASJI and the Sep–Oct WNPVI show insignificant correlation in 1979–2021, suggesting these two key circulation anomalies in the two seasons may be physically independent. In addition, observational and model hindcast suggests external forcings (e.g., SST, sea ice) played a limited role in this drought, indicating these two key circulation patterns leading to drought are primarily internally generated. Therefore, the persistence of this drought was probably caused by the relay effects of these two circulation patterns by chance.

5. Summary and Discussion

In summer–autumn of 2022, the YRB experienced an extreme meteorological drought, with YRBP in Jul–Oct 2022 the lowest since 1979, which coincided with a triple-dip La Niña event. In this study, we investigated the physical mechanisms of such a prolonged drought from the perspective of external forcing and internal variabilities. Our analysis demonstrated that circulation patterns responsible for drought in Jul–Aug and Sep–Oct 2022 show remarkable differences, indicating the drought may have disparate attributions in Jul–Aug and Sep–Oct, which should be discussed separately.

In Jul–Aug 2022, the tropical circulation anomaly featured a WNP anticyclone anomaly, which was unable to explain the YRBP deficit. Instead, extra-tropical circulation anomalies played an essential role. Specifically, mid-to-high latitude circulation anomalies over EA featured an intensified and northward-shifted EASJ, which allowed for the northwestward shift of WPSH and thus suppressed the YRBP. The SSTA, particularly the La Niña-like pattern, was able to explain the presence of the WNP anticyclone anomaly but unable to explain the observed YRB drought. Further analysis suggested the mid-to-high latitude circulation anomalies that caused the drought originated from different atmospheric teleconnections across the Eurasian continent, which implied the roles of atmospheric internal dynamics.

In Sep–Oct 2022, the YRB drought was primarily attributed to a low-level cyclonic anomaly over the WNP, while the impact from the upper-tropospheric circulation anomaly was relatively rigorous. The La Niña SST pattern was unable to explain the observed WNP cyclone anomaly, as a WNP anticyclone anomaly exists in Sep–Oct of the historical La Niña years. It was found that the frequent TCs traveling across the WNP region may have contributed to the development of an anomalous WNP cyclone, which obscured the response of the atmospheric teleconnection to La Niña forcing, i.e., the WNP anticyclone anomaly. Model ensemble hindcasts from CFSv2 suggest atmospheric internal variabilities dominated the drought process, while the SSTA played a limited role.

Therefore, this extreme YRB meteorological drought was largely driven by the relay effects of different atmospheric internal variabilities in Jul–Aug and Sep–Oct, respectively, which showed limited model predictability and posed a great challenge for operational climate predictions. The present study highlights that the random relay of different climate factors can act to extend drought duration, which provides a new vision for understanding the drought of 2022. However, several aspects of the physical mechanisms are still not clear. On the one hand, previous studies pointed out that a close teleconnection exists between the YRBP and the convection activity over the Indo-Pacific warm pool, i.e., a negative YRBP anomaly usually corresponds to decreased convection over the Maritime Continent and enhanced convection over the Philippines [31,32]. However, during the YRB drought of 2022, an opposite convection pattern, i.e., wet Maritime Continent and dry Philippines, was observed. It is still unclear why this extreme drought event was uncoupled with Indo-Pacific convection patterns, which requires further investigation in the future. On the other hand, the present study primarily focuses on the causes of a persistent precipitation deficit in the drought processes of 2022. It is also worth noting that in summer–autumn 2022,

the precipitation deficit co-occurred with a positive temperature anomaly, which would strengthen the severity of drought through increasing evaporation [33]. This implies a crucial role of the long-term warming trend in modulating the strength of YRB drought [34–36]. In future studies, through using large ensemble model simulations with anthropogenic forcing, the question of whether the concurrently dry and hot events analogous to the event in 2022 are likely to increase under global warming will be investigated.

Author Contributions: R.W., X.L. (Xiao Li) and H.M. contributed to the conception and design of the study. H.M., A.L. and J.W. organized the database. X.L. (Xing Li) and X.L. (Xiao Li) performed the statistical analysis. R.W., X.L. (Xiao Li) and H.M. wrote the first draft of the manuscript. A.L. and J.W. wrote sections of the manuscript. All authors have read and agreed to the published version of the manuscript.

Funding: This study was jointly supported by Joint Open Project of KLME & CIC-FEMD, NUIST (KLME202101, KLME202002), the Natural Science Foundation of Hubei Province (2022CFB983), Meteorological Joint Science and Technology Innovation Fund of Wuhan Metropolitan (WHCSQY202312), Basic Research Fund of WHIHR (202311), Hubei Meteorological Administration Scientific Project (2023Q03), and the National Natural Science Foundation of China (41905065).

Institutional Review Board Statement: Not applicable.

Informed Consent Statement: Not applicable.

Data Availability Statement: The monthly precipitation dataset from the GPCP) was downloaded from <https://psl.noaa.gov/data/gridded/data.gpcp.html>, accessed on 28 August 2023. The Centennial in situ Observation-Based Estimates of SST were downloaded from <https://psl.noaa.gov/data/gridded/data.cobe.html>, accessed on 28 August 2023. For the circulation variables, we used the NCEP-DOE atmospheric reanalysis dataset, which was available at <https://psl.noaa.gov/data/gridded/data.ncep.reanalysis2.html>, accessed on 28 August 2023.

Conflicts of Interest: The authors declare no conflict of interest.

References

1. Qiao, R.; Li, H.; Han, H. Spatio-temporal coupling coordination analysis between urbanization and water resource carrying capacity of the provinces in the Yellow River Basin, China. *Water* **2021**, *13*, 376. [CrossRef]
2. Ding, Y.H. Summer monsoon rainfalls in China. *J. Meteor. Soc. Jpn.* **1992**, *70*, 373–396. [CrossRef]
3. Xie, S.-P.; Kosaka, Y.Y.; Du, K.; Hu, J.; Chowdary, S.; Huang, G. Indo-western Pacific Ocean capacitor and coherent climate anomalies in post-ENSO summer: A review. *Adv. Atmos. Sci.* **2016**, *33*, 411–432. [CrossRef]
4. Wu, B.; Zhang, R.; Wang, B.; D’Arrigo, R. On the association between spring Arctic sea ice concentration and Chinese summer rainfall. *Geophys. Res. Lett.* **2009**, *36*, 666–678. [CrossRef]
5. Zhang, C.; Jia, X.; Wen, Z. Increased impact of the Tibetan Plateau spring snow cover to the Mei-yu rainfall over the Yangtze River valley after the 1990s. *J. Clim.* **2021**, *34*, 5985–5997.
6. Gao, C.; Li, G.; Xu, B.; Li, X. Effect of spring soil moisture over the Indo-China Peninsula on the following summer extreme precipitation events over the Yangtze River basin. *Clim. Dyn.* **2020**, *54*, 3845–3861. [CrossRef]
7. Qi, L.; Ji, Y.; Zhang, W. Indispensable Role of the Madden-Julian Oscillation in the 2019 Extreme Autumn Drought Over Eastern China. *J. Geophys. Res. Atmos.* **2021**, *126*, e2020JD034123. [CrossRef]
8. Li, X.; Lu, R.; Wang, X. Effect of Large-Scale Circulation Anomalies on Summer Rainfall over the Yangtze River Basin: Tropical versus Extratropical. *J. Clim.* **2023**, *36*, 4571–4587. [CrossRef]
9. Li, X.; Lu, R. Extratropical factors affecting the variability in summer precipitation over the Yangtze River basin, China. *J. Clim.* **2017**, *30*, 8357–8374. [CrossRef]
10. Wang, S.; Zuo, H.; Yin, Y.; Wang, J.; Ma, X. Asymmetric impact of East Asian jet’s variation on midsummer rainfall in North China and Yangtze River Valley. *Clim. Dyn.* **2019**, *53*, 6199–6213. [CrossRef]
11. Sampe, T.; Xie, S.-P. Large-scale dynamics of the meiyu-baiu rainband: Environmental forcing by the westerly jet. *J. Clim.* **2010**, *23*, 113–134. [CrossRef]
12. Ma, S.; Zhu, C.; Liu, J. Combined impacts of warm central equatorial Pacific sea surface temperatures and anthropogenic warming on the 2019 severe drought in East China. *Adv. Atmos. Sci.* **2020**, *37*, 1149–1163. [CrossRef]
13. Hua, W.; Dai, A.; Qin, M.; Hu, Y.; Cui, Y. How Unexpected Was the 2022 Summertime Heat Extremes in the Middle Reaches of the Yangtze River? *Geophys. Res. Lett.* **2023**, *50*, e2023GL104269. [CrossRef]
14. Tang, S.; Qiao, S.; Wang, B.; Liu, F.; Feng, T.; Yang, J.; Dong, W. Linkages of unprecedented 2022 Yangtze River Valley heatwaves to Pakistan flood and triple-dip La Niña. *npj Clim. Atmos. Sci.* **2023**, *6*, 44. [CrossRef]

15. Li, Z.; Xiao, Z. The role of Tibetan plateau–Indian Ocean thermal contrast in the significant increasing precipitation over the southern Tibetan plateau in may after the mid-1990s. *J. Clim.* **2022**, *35*, 7661–7675. [[CrossRef](#)]
16. Wang, Z.; Luo, H.; Yang, S. Different mechanisms for the extremely hot central-eastern China in July–August 2022 from a Eurasian large-scale circulation perspective. *Environ. Res. Lett.* **2023**, *18*, 024023. [[CrossRef](#)]
17. Jin, D.; Guan, Z.; Tang, W. The extreme drought event during winter-spring of 2011 in East China: Combined influences of teleconnection in mid-high latitudes and thermal forcing in Maritime Continent region. *J. Clim.* **2013**, *26*, 8210–8222. [[CrossRef](#)]
18. Wang, H.; He, S. The north China/northeastern Asia severe summer drought in 2014. *J. Clim.* **2015**, *28*, 6667–6681. [[CrossRef](#)]
19. Li, X.; Li, D.; Li, X.; Chen, L. Prolonged seasonal drought events over northern China and their possible causes. *Int. J. Climatol.* **2018**, *38*, 4802–4817. [[CrossRef](#)]
20. Zhang, L.; Wu, P.; Zhou, T.; Xiao, C. ENSO transition from La Niña to El Niño drives prolonged spring–summer drought over North China. *J. Clim.* **2018**, *31*, 3509–3523. [[CrossRef](#)]
21. Adler, R.F.; Huffman, G.J.; Chang, A.; Ferraro, R.; Xie, P.P.; Janowiak, J.; Nelkin, E. The version-2 global precipitation climatology project (GPCP) monthly precipitation analysis (1979–present). *J. Hydrometeorol.* **2003**, *4*, 1147–1167. [[CrossRef](#)]
22. Ishii, M.; Shouji, A.; Sugimoto, S.; Matsumoto, T. Objective analyses of sea-surface temperature and marine meteorological variables for the 20th century using ICOADS and the Kobe Collection. *Int. J. Clim.* **2005**, *25*, 865–879. [[CrossRef](#)]
23. Kanamitsu, M.; Ebisuzaki, W.; Woollen, J.; Yang, S.K.; Hnilo, J.J.; Fiorino, M.; Potter, G.L. NCEP-DOE AMIP-II Reanalysis (R-2). *Bull. Am. Meteor. Soc.* **2002**, *83*, 1631–1643. [[CrossRef](#)]
24. Ying, M.; Zhang, W.; Yu, H.; Lu, X.; Feng, J.; Fan, Y.; Zhu, Y.; Chen, D. An overview of the China Meteorological Administration tropical cyclone database. *J. Atmos. Ocean. Technol.* **2014**, *31*, 287–301. [[CrossRef](#)]
25. Bunge, L.; Clarke, A.J. A verified estimation of the El Niño index Niño-3.4 since 1877. *J. Clim.* **2009**, *22*, 3979–3992. [[CrossRef](#)]
26. Takaya, K.; Nakamura, H. A formulation of a phase-independent wave-activity flux for stationary migratory quasigeostrophic eddies on a zonally varying basic flow. *J. Atmos. Sci.* **2001**, *58*, 608–627. [[CrossRef](#)]
27. Xuan, S.; Zhang, Q.; Sun, S. Anomalous midsummer rainfall in Yangtze River-Huaihe River valleys and its association with the East Asia westerly jet. *Adv. Atmos. Sci.* **2011**, *28*, 387–397. [[CrossRef](#)]
28. Li, L.; Zhang, Y. Effects of different configurations of the East Asian subtropical and polar front jets on precipitation during the mei-yu season. *J. Clim.* **2014**, *27*, 6660–6672. [[CrossRef](#)]
29. Zhang, W.; Jin, F.F.; Turner, A. Increasing autumn drought over southern China associated with ENSO regime shift. *Geophys. Res. Lett.* **2014**, *41*, 4020–4026. [[CrossRef](#)]
30. Hu, P.; Chen, W.; Chen, S.; Liu, Y.; Huang, R.; Dong, S. Relationship between the South China Sea summer monsoon withdrawal and September–October rainfall over southern China. *Clim. Dyn.* **2020**, *54*, 713–726. [[CrossRef](#)]
31. Li, C.; Scaife, A.A.; Lu, R.; Arribas, A.; Brookshaw, A.; Comer, R.E.; Wu, P. Skillful seasonal prediction of Yangtze river valley summer rainfall. *Environ. Res. Lett.* **2016**, *11*, 094002. [[CrossRef](#)]
32. Shen, B.; Yang, Y.; Chen, Q. Precipitation prediction during flood season in the Yangtze River Basin based on interannual increment and EOF iteration method. *Torrential Rain Disasters* **2022**, *41*, 651–661. (In Chinese)
33. Zhang, Y.; You, Q.; Mao, G.; Chen, C.; Li, X.; Yu, J. Flash drought characteristics by different severities in humid subtropical basins: A case study in the Gan River Basin, China. *J. Clim.* **2021**, *34*, 7337–7357. [[CrossRef](#)]
34. Williams, A.P.; Seager, R.; Abatzoglou, J.T.; Cook, B.I.; Smerdon, J.E.; Cook, E.R. Contribution of anthropogenic warming to California drought during 2012–2014. *Geophys. Res. Lett.* **2015**, *42*, 6819–6828. [[CrossRef](#)]
35. Hoell, A.; Perlwitz, J.; Dewes, C.; Wolter, K.; Rangwala, I.; Quan, X.W.; Eischeid, J. Anthropogenic contributions to the intensity of the 2017 United States northern great plains drought. *Bull. Amer. Meteor. Soc.* **2019**, *100*, S19–S24. [[CrossRef](#)]
36. Chen, L.; Li, Y.; Ge, Z.A.; Lu, B.; Wang, L.; Wei, X.; Luo, J.J. Causes of the Extreme Drought in Late Summer–Autumn 2019 in Eastern China and Its Future Risk. *J. Clim.* **2023**, *36*, 1085–1104. [[CrossRef](#)]

Disclaimer/Publisher’s Note: The statements, opinions and data contained in all publications are solely those of the individual author(s) and contributor(s) and not of MDPI and/or the editor(s). MDPI and/or the editor(s) disclaim responsibility for any injury to people or property resulting from any ideas, methods, instructions or products referred to in the content.